



Visible-light photocatalysis accelerates As(III) release and oxidation from arsenic-containing sludge



Hongbo Lu^{a,b}, Xueming Liu^c, Feng Liu^a, Zhengping Hao^{a,b}, Jing Zhang^{a,b,*}, Zhang Lin^c, Yvonne Barnett^d, Gang Pan^{a,e}

^a Key Laboratory of Environmental Nano-technology and Health Effect, Research Center for Eco-Environmental Sciences, Chinese Academy of Sciences, Beijing 100085, PR China

^b National Engineering Laboratory for VOCs Pollution Control Materials & Technology, University of Chinese Academy of Sciences, Beijing 101408, PR China

^c School of Environment and Energy, South China University of Technology, Guangzhou 510006, PR China

^d School of Science and Technology, Nottingham Trent University, Clifton Campus, NG11 8NS, UK

^e Centre of Integrated Water-Energy-Food Studies (iWEF), School of Animal, Rural, and Environmental Sciences, Nottingham Trent University, Brackenhurst Campus, NG25 0QF, UK

ARTICLE INFO

Keywords:
Arsenic sulfide sludge
Photocatalysis
Release
Oxidation
Active free radicals

ABSTRACT

Arsenic containing sludge, a product of the treatment of acid smelting wastewater, is susceptible to temperature, pH, co-existing salt ions and organic matter, which might lead to the release of arsenic ions into the environment. Here, we studied the effect of visible light on the dissolution and oxidation of arsenic sulfide sludge (ASS) sampled from a smelting plant. Results show that by exposure to visible light, both the release of As(III) ions from ASS and the oxidation of As(III) into As(V) were markedly accelerated. Electron paramagnetic resonance (EPR) and free radical quenching experiments revealed that ASS acts as a semiconductor photocatalyst to produce hydroxide and superoxide free radicals under visible light. At pH 7 and 11, both the dissolution and the oxidation of the sludge are directly accelerated by $\cdot\text{O}_2^-$. At pH 3, the dissolution of the sludge is promoted by both $\cdot\text{O}_2^-$ and $\cdot\text{OH}$, while the oxidation of As(III) is mainly controlled by $\cdot\text{OH}$. In addition, the solid phase of ASS was transformed to sulfur (S_8) which favored the aggregation and precipitation of the sludge. The transformation was affected by the generation of intermediate sulfur species and sulfur-containing free radicals, as determined by ion chromatography and low-temperature EPR, respectively. A photocatalytic oxidation-based model is proposed to underpin the As(III) release and oxidation behavior of ASS under visible light conditions. This study helps to predict the fate of ASS deposited in the environment in a range of natural and engineered settings.

1. Introduction

Arsenic is ubiquitous in the Earth's crust, with a mean concentration of 0.5–2.5 mg/kg – about 0.00005% of the Earth's crust [1]. It often coexists with the ores containing precious and non-ferrous metals, or iron [2]. During metal smelting, mineral processing, and sulfuric acid production from pyrite ores, a large amount of arsenic-containing acid wastewater and tailings are produced [3]. For example, the arsenic concentration in the wastewater from a sulfuric acid plant can range from several to tens of thousands mg/L [4]. One of the most popular techniques for treatment of the arsenic wastewater in industry is sulfide precipitation, where sulfide is employed to transform arsenic ions into arsenic sulfide precipitate [5]. This technique has many advantages,

such as low solubility of arsenic sulfide at a low pH, high sediment rate and efficiency, less sludge volume and water content [6,7]. As a result, large quantities of arsenic sulfide slag is discharged into the environment. For example, more than half a million tons of arsenic sludge are produced annually in China.

Arsenic sulfide sludge deposited in the environment is susceptible to temperature, pH, coexisting organics and inorganics (e.g. sulfides) [8,9]. The weathered and dissolved residues promote the release of arsenic ions into the surroundings, which can result in the transport and transformation of chemical species (e.g. arsenic and sulfur) in natural waters and so leading to environmental contamination. Previous studies have demonstrated that when pH is higher than 9, the dissolution of artificial As_2S_3 particles is significantly enhanced, owing to the

Abbreviations: ASS, arsenic sulfide sludge

* Corresponding author at: Key Laboratory of Environmental Nano-technology and Health Effect, Research Center for Eco-Environmental Sciences, Chinese Academy of Sciences, Beijing 100085, PR China.

E-mail address: jingzhang@rcees.ac.cn (J. Zhang).

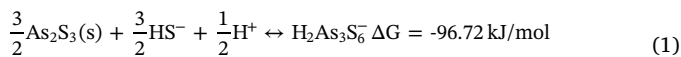
<https://doi.org/10.1016/j.apcatb.2019.03.020>

Received 23 December 2018; Received in revised form 21 February 2019; Accepted 8 March 2019

Available online 08 March 2019

0926-3373/© 2019 Elsevier B.V. All rights reserved.

enhanced activity of the hydroxylated surface species [10]. On the other hand, different types of sulfur species can influence the dissolution rate of arsenic sulfide. For instance, the added sulfide ions can react with arsenic sulfide and produce arsenic-sulfide complex ($\text{H}_2\text{As}_2\text{S}_6^-$), according to eq 1, which will accelerate the dissolution of the solid [11,12].



Recently, the effect of light on the dissolution of minerals containing heavy metals has been studied to elucidate the mechanism of photo-corrosion reactions on the release of metal ions, such as antimony and vanadium, from their parental minerals or the synthesized substitutes (e.g. senarmontite (Sb_2O_3) [13], stibnite (Sb_2S_3) [14], and vanadium titano-magnetic [15]). It has been demonstrated that simulated sunlight or UV irradiation can promote the dissolution of minerals and thus release heavy metal ions. Up to this time, no work has been reported on the effect of light-induced photochemical reactions on the fate of actual arsenic sludge from industry. As sunlight is one of the most important climate factors for ecosystems, it inevitably affects the fate of heavy metal slag deposited in the environment. On the other hand, arsenic sulfide is a semiconductor with a band gap (~2.34 eV) in the range of visible light spectrum. It has been reported that photocorrosion of artificial As_2S_3 colloids could occur by light irradiation [16]. Therefore, it is expected that the actual sludge, which mainly contains arsenic sulfide, is photo-responsive under visible light conditions.

The objective of the investigations described in this paper was to study the dissolution and transformation mechanisms of actual arsenic-containing sludge under visible light conditions. The release and oxidation kinetics of arsenic and sulfur from the sludge, as well as the structure and state of the solid phase, were examined at different pHs under visible light. The intermediate sulfur species arising during the photoreactions were quantified by ion chromatography. The photo-generated active oxygen and sulfur species were identified by EPR and free radical quenching experiments, and their specific contributions to the transformation of the sludge are discussed. The findings of the present investigation assist in the understanding of the fate and transforming process of arsenic sulfide sludge in the environment.

2. Materials and methods

2.1. Chemicals and materials

The details of all reagents used are provided in the Supporting Information. The arsenic sulfide sludge, a product of acid wastewater treatment, was sampled from a smelting plant in Fujian province, China.

2.2. Photo reaction system

All the photo reactions were performed in a 250 mL beaker by mixing 0.15 g of the solid sludge with 225 g of H_2O . The concentration of ASS was fixed at 0.67 g/L. The initial pH of the suspension was adjusted with HCl or NaOH solution. A 500-W Xe arc lamp (Shanghai Jiguang Special Lighting Appliance Factory, China) was used as a light source equipped with UV cut filters ($\lambda > 420 \text{ nm}$). The temperature for all the reactions was room temperature (RT ~25 °C) using a water-cooling system. At the appropriate time interval, the liquid samples were taken out and filtered through a 0.25 μm filter for further analysis. The dissolved oxygen level was controlled by using a gas-purging tube to inject N_2 or O_2 in the system. In order to study the effects of active species, specific radical scavengers were individually added into the reactor, including 0.1 M tert-butyl alcohol (TBA) for scavenging $\cdot\text{OH}$, 0.1 M methanol (MeOH) for SO_4^{2-} , and 1 mM p-benzoquinone (p-BQ) for $\cdot\text{O}_2^-$.

2.3. Analytical methods

2.3.1. Arsenic and sulfur species in the liquid phase

The concentration of As(V) was determined using the colorimetric molybdate blue method, and the total As ions (TAs) were measured after As(III) was oxidized completely by KMnO_4 [17]. S(II) species, including H_2S , HS^- , and S^{2-} , were analyzed using the methylene blue method [18]. The concentration of total sulfur (TS) was measured on an ICP-OES (OPTIMA 8300, PerkinElmer, USA). The quantification of sulfur intermediates, including sulfate (SO_4^{2-}), thiosulfate ($\text{S}_2\text{O}_3^{2-}$), and sulfite (SO_3^{2-}), was determined using an ion chromatograph (IS-2000) equipped with a Dionex IonPac™ AS19 (250 × 4 mm) column. The details of instrumental setups were described in the SI (Table S1).

2.3.2. Solid phase of the sludge

High-resolution field emission transmission electron microscopy (HRTEM) (JEM-2100 F, Japan) and scanning electron microscopy (SEM) (SU8020, Japan) were used to characterize the surface morphology of the solids. X-ray diffraction (XRD) (PANalytical B.V.X'Pert3 Powder) featuring a Cu – K (alpha) source was used to determine the crystal phases of samples. X-ray photoelectron spectroscopy (XPS) was performed on an ESCALAB 250Xi instrument (Thermo Fisher Scientific). The As 3d and S 2p XPS spectra were fitted by the XPSPEAK41 software. A UV-2600 spectrometer was used to determine the UV-vis absorption spectra of arsenic sludge. X-ray fluorescence (XRF) was performed on an Axios instrument PW4400 (PANalytical B.V.).

2.3.3. EPR analysis of active free radicals

$\cdot\text{O}_2^-$, $\cdot\text{OH}$ and SO_3^- radicals were detected on a Bruker EleXsys EPR spectrometer (A300-10/12, Germany) at RT with DMPO as the spin-trapping agent under visible light. When detecting $\cdot\text{O}_2^-$, the methanol was chosen as the dispersion. The sulfur-containing radicals were detected on a Bruker EleXsys EPR spectrometer (E500, Germany) at the low temperature (90 K) using a 100 W mercury lamp equipped with UV cut filters (2000 nm > λ > 420 nm) [19].

3. Results and discussion

3.1. Analysis of raw ASS

The XRD pattern of ASS revealed that the sludge mainly contained nanosized and amorphous As_2S_3 particles plus some undefined impurities (Fig. 1a). The SEM image in Fig. 1b also shows that the sludge comprised of small particles with the size less than 100 nm. HRTEM image (Figs. 1b and S1) further confirmed that the particles are amorphous structure. EDS mapping images revealed that the two components, As and S, overlapped each other (Fig. 1d). The XRF and ICP-OES results (Table S2) confirm that As and S accounted for the two main components of ASS (more than 80% in mass), while other elements, such as Na, Ni, and Cu, accounted for only 4.18% of the total.

XPS spectra (Fig. 1c) of ASS show that the peaks observed ranging from 41 to 47 eV, identified as two separated peaks at 43.40 and 44.10 eV (the intensity ratio 5:3), which are ascribed to As 3d_{5/2} and As 3d_{3/2} of As(III), respectively [20]. No As(V) was detected in the system. The peaks from 161 to 170 eV are corresponding to S 2p, which can be fitted by three groups of peaks [21–23]. Each group with a separation of 1.2 eV and the intensity ratio of 2:1, is assigned to S 2p_{3/2} and S 2p_{1/2}. The first group of peaks (1-1' in Fig. 1c) located at 162.5 and 163.7 eV originate from S^{2-} , while the second pairs (2-2' in Fig. 1c) at 163.2 and 164.4 eV are from S_2^{2-} . The third group of peaks at 169.0 and 170.2 eV correspond to SO_4^{2-} , indicating that sulfur ions in the sludge were partially oxidized [24].

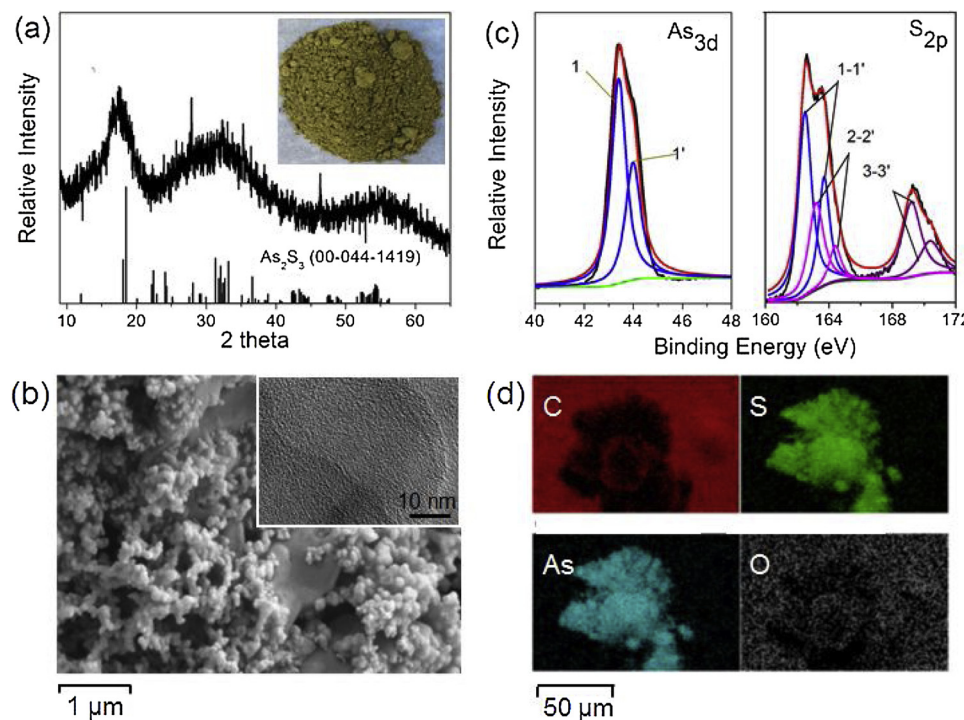


Fig. 1. (a) XRD pattern, (b) SEM image with the inserted HRTEM image, (c) XPS spectra, and (d) EDS mapping images of the raw sludge. In the As 3d spectra, 1 and 1' are assigned to As 3d_{5/2} and As 3d_{3/2}, respectively. In the S 2p spectra, 1–3 are assigned to S 2p_{3/2}, and 1', 2', 3' are from S 2p_{1/2} of S²⁻ (1-1'), S₂²⁻ (2-2') and SO₄²⁻ (3-3'). Inset of (a): optical image of the sludge.

3.2. Arsenic release from ASS under visible light

The total dissolved arsenic concentration, as a function of time for ASS in aqueous solution at different pH values, is shown in Fig. 2a. Without light irradiation, the total arsenic ions (TAs) in solution at pH 3 and pH 7 had a low concentration, increasing slightly with time. Approximately 8 ppm of TAs could be detected after 5 h at both pH values. At pH 11, TAs in the solution quickly increased with time and reached a plateau after 1 h, where the TAs concentration was about 3 times of that at the low pH. These kinetic observations share similar trends with the results of ref 14, in which the solubility of artificial As₂S₃ particles was independent of pH before pH 6, after which the concentration of TAs increased with pH (as expressed by Eq. (1)).

Under visible light irradiation, the dissolution rate of the sludge markedly increased at all the three pH values, as compared to the corresponding cases in the dark. At each pH, the concentration of TAs increased with time, which showed a linear increase after 10 min. On the basis of linear fit (Fig. S2), the dissolution rates of ASS at pH 3, 7 and 11 were 12.61, 11.18, and 12.14 ppm/h, respectively. These data indicated that the illumination by visible light ($\lambda > 420$ nm) can greatly promote the release of arsenic ions from ASS. Moreover, the increase of TAs concentration by light was more pronounced at lower pH. Specifically, the TAs concentration after light irradiation for 5 h was about 8.2, 6.9, and 3.1 times higher, compared to the dissolution in the dark, from low to high pH. These results imply that the light-promoted dissolution of ASS is controlled by the different mechanisms at varied pH values (see the discussion in the Section 3.7).

3.3. Arsenic oxidation of ASS under visible light

The concentration of As(V) ions were also measured to check the oxidation of ASS under visible light irradiation. As shown in Fig. 2b, in the dark, almost no As(V) at pH 3 and pH 7, while at pH 11, the concentration of As(V) quickly increased to 4.5 ppm at 30 min and then remained at equilibrium. These findings indicated that the oxidation of As(III) into As(V) by oxygen was favored in a basic solution, probably due to the lower redox potential of As(III)/As(V) at higher pH [25].

Under visible light, the concentration of As(V) at pH 3 and pH 7

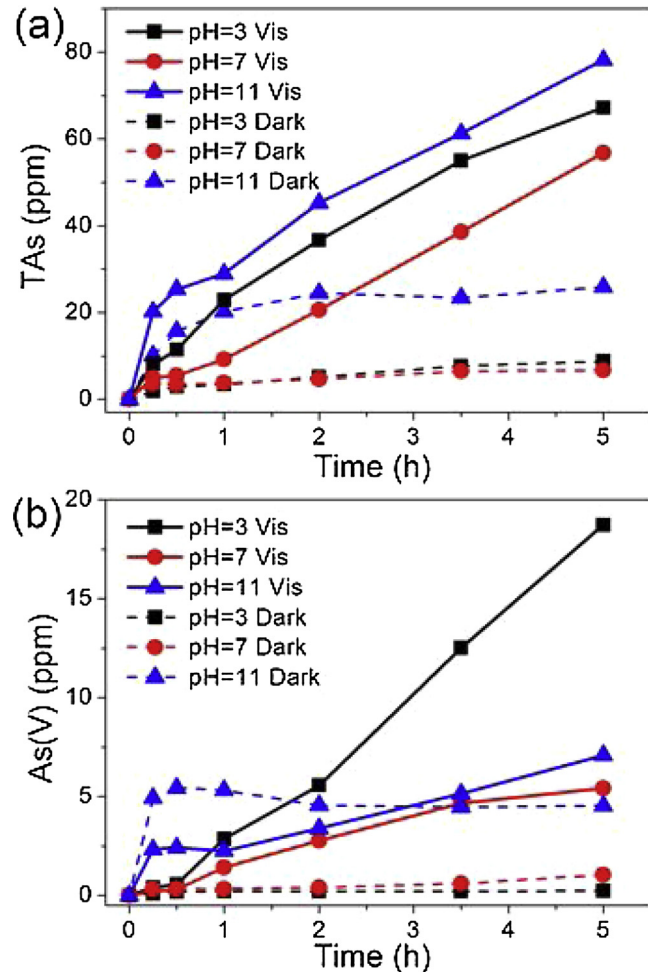


Fig. 2. Dissolution and oxidation of the sludge in water at different pHs under visible light irradiation (vis): (a) the release rate of total As (TAs) and (b) the oxidation rate of As(III).

increased with time in a roughly linear mode. Moreover, the oxidation rate of As(III) at pH 3 was much faster than the rate at pH 7 and pH 11. After 5 h of irradiation, the concentration of As(V) at pH 3 was 79.8 times higher than that in the dark, as compared to 5.2 and 1.2 times at pH 7 and pH 11, respectively. By linear fit (Fig. S2), the oxidation rates of ASS at pH 3, 7 and 11 were 3.92, 1.16, and 1.02 ppm/h, respectively. These data suggest that the oxidation of As(III) into As(V) is accelerated by light illumination, and more so under acid conditions (see the discussion in the Section 3.8). It was notable that at pH 11, a lower concentration of As(V) was obtained at the beginning under visible light than that in the dark. This is probably due to the decrease of pH during the rapid dissolution of ASS under illumination (Table S3), which could change the redox potential of As(III)/As(V) [25]. But with time, the oxidation of As(III) by light was the dominant factor.

In addition, the effects of the ASS concentration on the dissolution and oxidation efficiency were checked (Fig. S3). The results indicated that the dissolution and oxidation efficiency of ASS was proportional to the amount of the sludge.

3.4. Solid state of ASS after illumination

Fig. 3a shows that the XRD patterns of ASS remained almost the same under the different pH conditions when in the dark and still kept the characteristic peaks of As_2S_3 . However, an obvious change could be observed after illumination, where the broad peaks from As_2S_3 were suppressed and new sharp peaks occurred (Fig. 3b). The new phase could be identified as S_8 (JCPDS NO.00-044-1419). The species in the ASS with and without visible light irradiation were further characterized by XPS. As shown in Fig. S4, two group of peaks (1-1' and 2-2') located at the binding energies of 162.4–163.6 eV (1-1') and 163.2–164.4 eV (2-2') are corresponding to S 2p of S^{2-} and S_2^{2-} , respectively. But after light irradiation, the ratio of two group peaks for all pH values decreased, indicating that new S species were produced. By fitting the spectra, the peaks can be deconvoluted into two new additional peaks at 163.9 and 165.1 eV (3-3'), which are assigned to S 2p_{1/2} and S 2p_{3/2} of S° , respectively [21–23]. The XPS results confirm the production of S_8 , which is coincident with the XRD data. From the XPS fitting results (Table S4), the contents of S_8 in the total S after light irradiation were obtained as 14.1%, 10.2%, and 15.2%, at pH 3, 7, and 11, respectively. These data revealed the same pH-dependent order as the dissolution of total arsenic from ASS under illumination, which suggests that the release of arsenic ions from the sludge is accompanied with the generation of S_8 .

The precipitation state of ASS in aqueous solution after visible light irradiation was checked and compared with the case without illumination. As shown in Fig. 3c, after 5 h of irradiation the sludge quickly settled down within 2 min and a clear supernatant solution was obtained. Without light irradiation the particles were highly suspended in the solution and complete precipitation could only be achieved after sitting for two days. A great improvement in the sedimentation performance can be reasonably ascribed to both an increase of the particle size and the change of particle surface properties, where the hydrophobic S_8 produced on the surface of the sludge promotes particle aggregation and sedimentation [26].

3.5. Sulfur speciation released in the solution

As mentioned above, not only the release and oxidation of As from ASS, but also the phase transformation from As_2S_3 to S_8 , are accelerated under visible light irradiation. To get a better understanding of the transition of sulfur during the dissolution of ASS, the sulfur species in the system were monitored.

Fig. 4a shows that the concentration of Total Sulphur (TS) in the solution increased with pH increasing without light irradiation, where a distinctive increase can be seen at pH 11. These data demonstrated similar trends with the pH-dependent release of arsenic in solution.

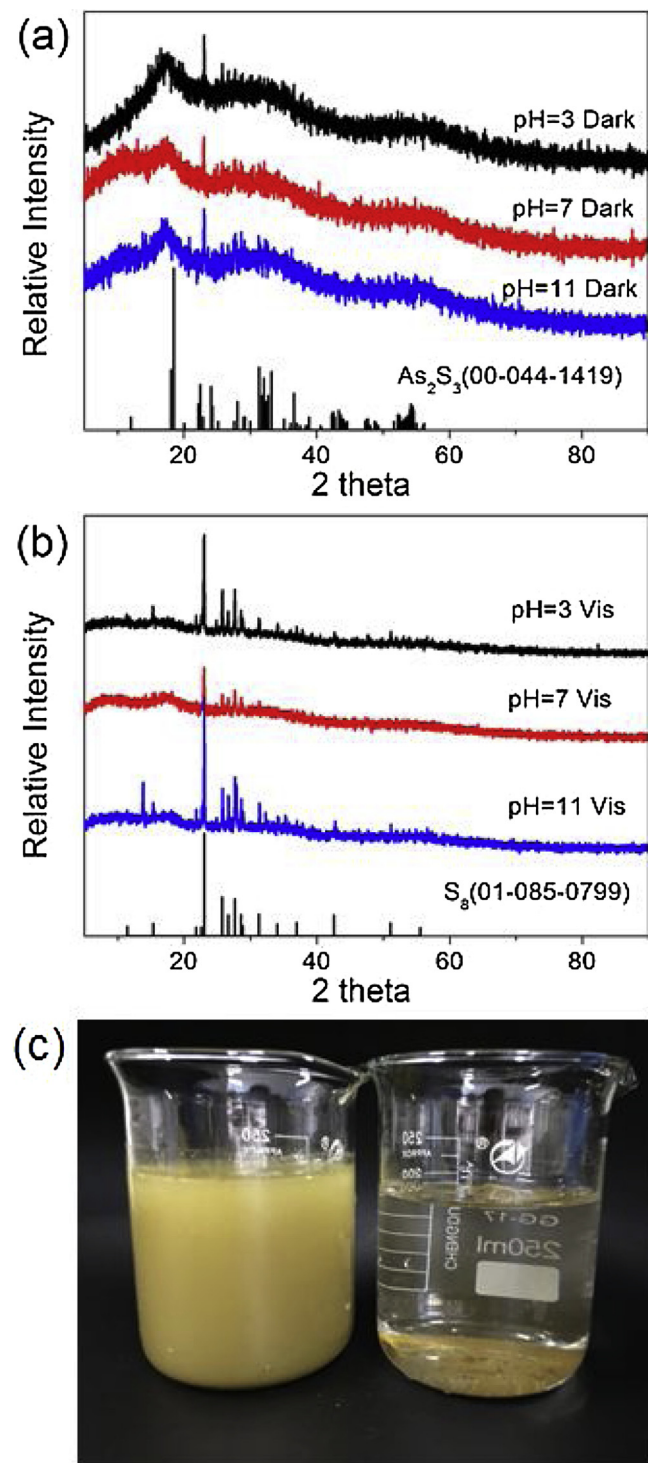


Fig. 3. XRD patterns of the sludge (a) in the dark and (b) under visible light after 5 h. (c) Photo of the sludge in water without light irradiation and sitting for two days (left), and under 5 h of visible light irradiation and standing for 2 min (right).

Under visible light illumination the release of TS was accelerated at all pH values. However, there was only a limited increase of TS at pH 3 and 7, while at pH 11, a distinct increase of about 25 ppm/S was observed after 2 h of light illumination, as compared to that in the dark.

Specifically, the sulfur species, including SO_4^{2-} , S^{2-} , SO_3^{2-} and $\text{S}_2\text{O}_3^{2-}$, were detected under visible light (Fig. 4b and c). At pH 3, SO_4^{2-} increased quickly with time and dominated in solution, accounting for about 50% (15.6 ppm/S) of TS at equilibrium. The reduced

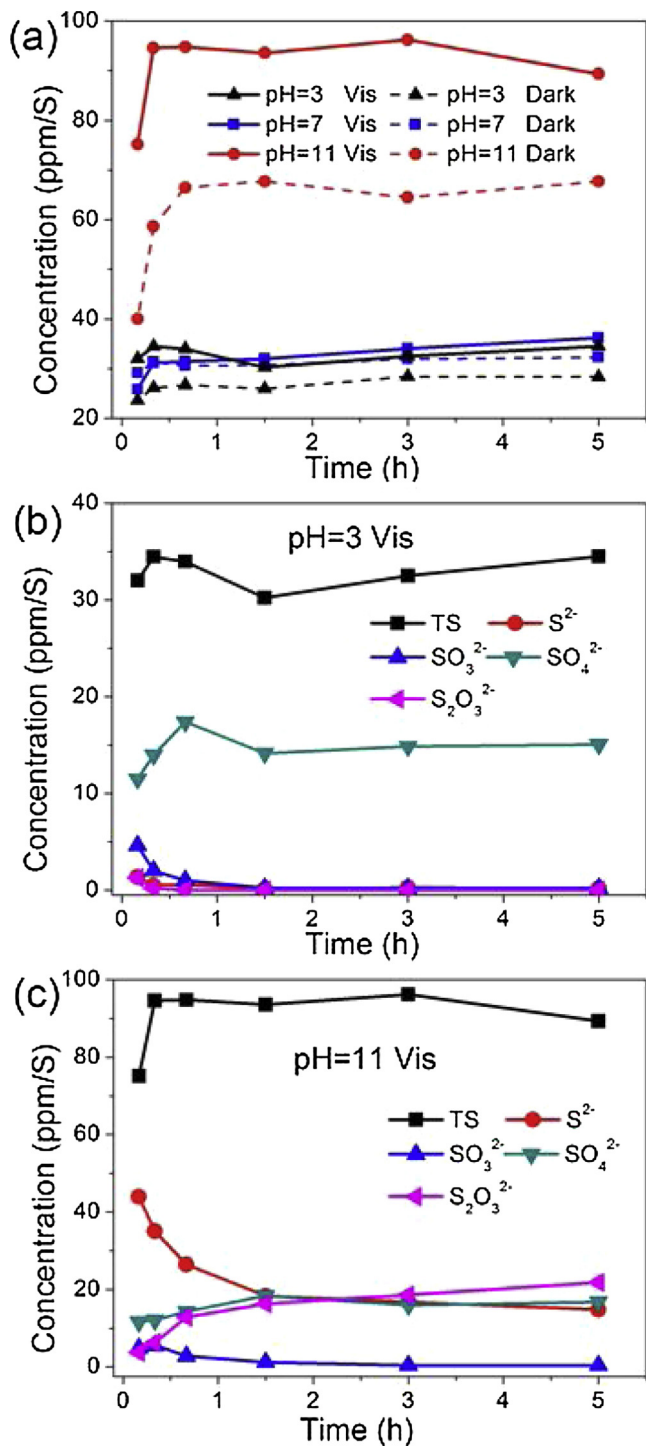


Fig. 4. (a) Release rate of total sulfur (TS) under visible light irradiation at different pHs. (b and c) Release rate of different sulfur species (TS, S²⁻, SO₃²⁻, SO₄²⁻, and S₂O₃²⁻) at pH 3 (b) and pH 11 (c).

and intermediate sulfur species, such as S²⁻ and SO₃²⁻ and S₂O₃²⁻, decreased to a very low concentration with time. These data suggest that sulfur might be first dissolved in the form of reduced sulfur species and finally oxidized into SO₄²⁻. It is worth noting that the concentration of TS was higher than the sum of all the detected S species, probably due to the reason that other sulfur species, such as polythionates (S_nO₆²⁻, n = 3, 4, 5 or 6) [27], were not able to be separated or detected. At pH 11, SO₄²⁻, S²⁻ and S₂O₃²⁻ had an equivalent concentration (~20 ppm/S) and these three species mainly contributed to

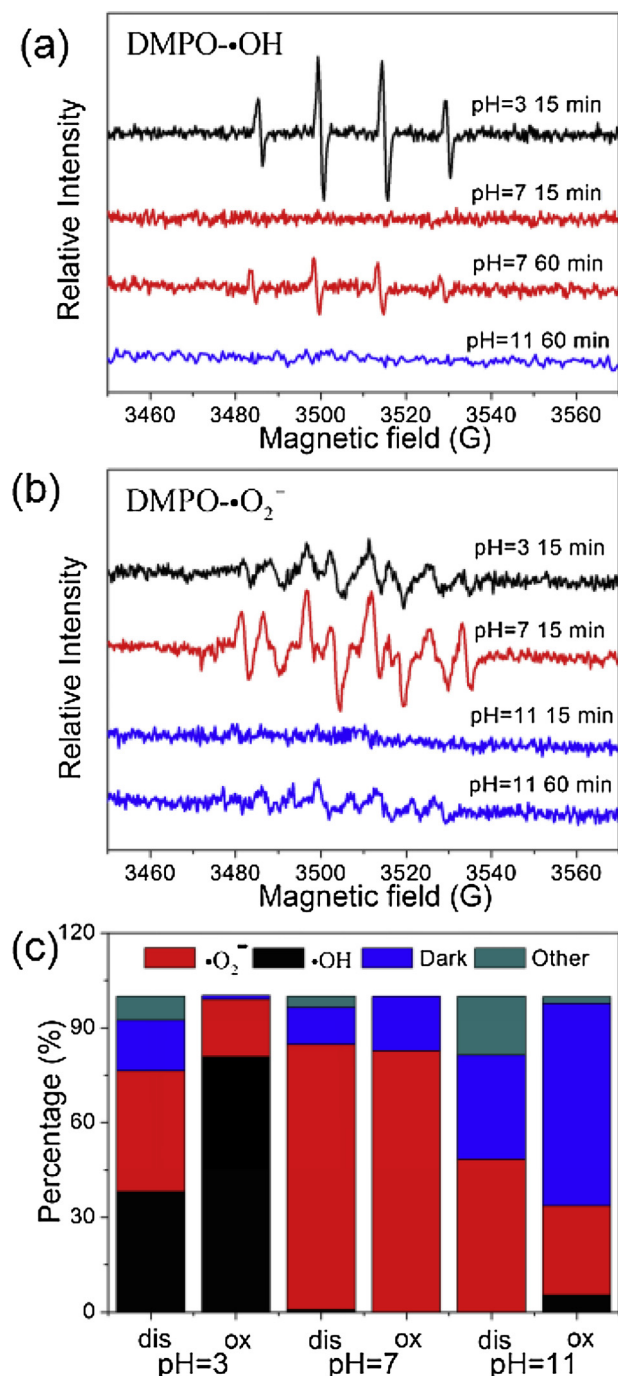


Fig. 5. EPR spectra of (a) DMPO-·OH and (b) DMPO-·O₂⁻ produced by light irradiation at different pH (Measurement conditions: 25 mM DMPO and RT), and (c) Contribution ratio of dissolution (dis) and oxidation (ox) of the sludge by ·OH and ·O₂⁻ after 5 h of light irradiation at different pH (calculated from the concentration of TAs and As(V)).

the TS. Comparing to sulfur species at pH 3, a higher concentration of S²⁻ and S₂O₃²⁻, can be found at pH 11. This indicates that the sulfur oxidation under light irradiation in the basic solution is less favorable than that in the acid condition, which is consistent with the arsenic oxidation at different pH values.

3.6. Evaluation of photo-generated active oxygen species

It is known that As₂S₃ is a semiconductor with a band gap of 2.34 eV. In the ASS investigated, the measured band gap was 1.89 eV

(Fig. S5), indicating a strong absorption and photocatalytic activity in visible light region. Therefore, under visible light irradiation the ASS could generate photo-generated holes (h_{vb}^+) and electrons (e_{cb}^-) (Eq. (2)), which will further react with the species, such as oxygen, hydroxide, and sulfur, to produce active free radicals.



EPR was used to directly evidence the generation of the involved free radicals in ASS under visible light irradiation. As shown in Fig. 5a, at pH 3, a strong DMPO-·OH [28] signal could be clearly observed by illumination for 15 min. At pH 7, only a weak DMPO-·OH signal appeared even after illumination for 1 h. But at pH 11, no signal of hydroxyl radical was detected. These data indicate that the concentration of ·OH decreased with the increase of pH values. Meanwhile, the superoxide radical was also monitored and as shown in Fig. 5b, the characteristic peaks of the DMPO-·O₂[·] [29,30] were detected at all three pH values, although the intensities from ·O₂[·] at pH 3 and pH 7 were stronger than that at pH 11. Notably, in the dark, neither ·O₂[·] nor ·OH was detected in the all corresponding systems (Fig. S6).

On the basis of photocatalytic mechanism, normally ·OH can be produced in two ways, one of which is directly generated from h_{vb}^+ : [31,32]



The other way is from e_{cb}^- in the presence of O₂ via a multistep reaction: [33,34]



It can be seen from the above reactions that ·OH generated from h_{vb}^+ is more favorable in a neutral or basic condition, while a low pH and dissolving oxygen help to produce ·OH from e_{cb}^- . From our EPR results that show a higher concentration of ·OH obtained at the low pH, it can be deduced that ·OH in the system is probably generated via ·O₂[·] in the multistep reaction shown above.

3.7. The effects of ·O₂[·] and ·OH on arsenic release

In order to study the effect of different free radicals on the dissolution and oxidation of ASS, TBA and p-BQ were used as the scavengers to quench ·OH and ·O₂[·], respectively [35,36]. As shown in Fig. 6a–c, in the presence of p-BQ (·O₂[·] quencher), the release of TAs from ASS was effectively suppressed at all three pH values. When TBA (·OH quencher) was added, TAs release was partially inhibited at pH 3 (~33% cut), and with pH increasing, the inhibitory effect was decreased and hardly observed at pH 11. The results revealed that both ·OH and ·O₂[·] contributed to the release of TAs at pH 3, but only ·O₂[·] contributed at the high pH 7 and pH 11. Their contributions are summarized in Fig. 5c.

As discussed above (Eqs. (5)–(9)), ·OH was generated from ·O₂[·] in the system, which means that the dissolution of arsenic from the sludge basically originates from the contribution of ·O₂[·]. So when p-BQ was added in the system at pH 3, most of the dissolution of TAs was suppressed, because the scavenger can both directly inhibit ·O₂[·] and indirectly eliminate ·OH that originally stemmed from ·O₂[·].

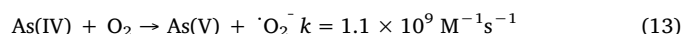
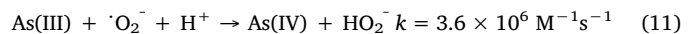
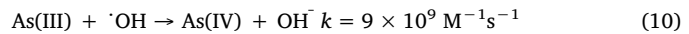
The effects of reactive oxygen species on accelerating the dissolution of ASS were further proved by purging O₂ or N₂ in the systems (Fig. S7). The released TAs were obviously increased by purging O₂ at all

three pH values, while suppressed by purging N₂ in the solution, although a simply purging N₂ failed to achieve an anoxic condition through completely excluding the dissolved oxygen.

3.8. The effects of ·O₂[·] and ·OH on arsenic oxidation

As shown in Fig. 6d–f, the effects of ·O₂[·] and ·OH on the oxidation of As(III) into As(V) shared similar trends with the release of arsenic from the sludge (Fig. 6a–c). At pH 3, both TBA and p-BQ reduced the concentration of As(V) close to zero, suggesting that the oxidation of the released As(III) is effectively suppressed. At the high pH values (7 and 11), TBA had little impact on the concentration of As(V), but p-BQ suppressed almost all the production of As(V). The contributions of different radicals to the oxidation of As(III) is summarized in Fig. 5c. It demonstrates that both ·OH and ·O₂[·] can oxidize As(III) into As(V). But at the low pH, ·OH contributed more to the oxidation of As(III). As ·OH has a higher oxidation potential than ·O₂[·], more As(V) was thus obtained at pH 3 (Fig. 2b), even if the concentration of total arsenic ions released in the solution was less than that at pH 11 (Fig. 2a). As discussed before, TBA directly scavenges ·OH, while p-BQ consumes ·O₂[·] and thus indirectly inhibits the generation of ·OH. Our results reveal that ·O₂[·] is the critical radical in the system and controls the oxidation of As(III).

The pathway of As(III) being oxidized into As(V) is proposed as follows (Eqs. (10)–(13)): [37,38]



During the oxidation process, As(IV) is the intermediated arsenic species, which will finally transform to As(V) via a As(IV) disproportionation reaction (Eq. (12)) or by further oxidizing with the dissolved O₂ (Eq. (13)) [38]. From Eqs. (10) and (11), it can be seen that the oxidation rate of As(III) by ·OH is much higher than ·O₂[·]. So, the concentration of As(V) at pH 7 and 11 is obviously smaller than that at pH 3. However, the oxidation-reduction potential of As(V)/As(III) also decreases with the increase of pH values [25]. For example, $E^\circ(\text{As(V)/As(III)})$ at pH 3 and pH 9 are 0.40 V and -0.2 V, respectively [39]. This will provide the chance for ·O₂[·], as a weak oxidant, to directly oxidize As(III) at high pH, when ·OH is in short. It has been reported that superoxide radicals can act as the main free radicals to oxidize arsenic at pH 9 [39,40]. Combining with the results from the quenching experiments (Fig. 6e and f), it can be reasonably deduced that ·O₂[·] is responsible for the oxidation of As(III) at pH 7 and 11 in our system.

3.9. Photo-generated active sulfur radicals and their effects on the production of S₈

Visible light irradiation not only accelerates the release and oxidation of As(III) from ASS, but also promotes the production of sulfur-related ions and the solid phase S₈. In order to understand the transformation of sulfur species and their effects on the dissolution of ASS, active sulfur species that are expected to form under light illumination, were monitored by EPR at 90 K. As shown in Fig. 7a, multiple peaks located at the magnetic field of 3150–3400 G were observed at all three pH values. These were sulfur-containing free radicals, S[·]_(s), at $g = 2.052\text{--}2.021$ [41,42] and sulfur-oxide anion radicals, SO₂[·]⁻, at $g = 2.003$ [19]. Normally, sulfide containing radicals are difficult to capture in an aerobic environment, due to readily reacting with oxygen and thus having an extremely short lifetime [19]. Also, the radicals are very sensitive to temperature and the measured spectra gradually diminish on warming. Thus, the measurement has to be done at a low temperature (90 K in our case).

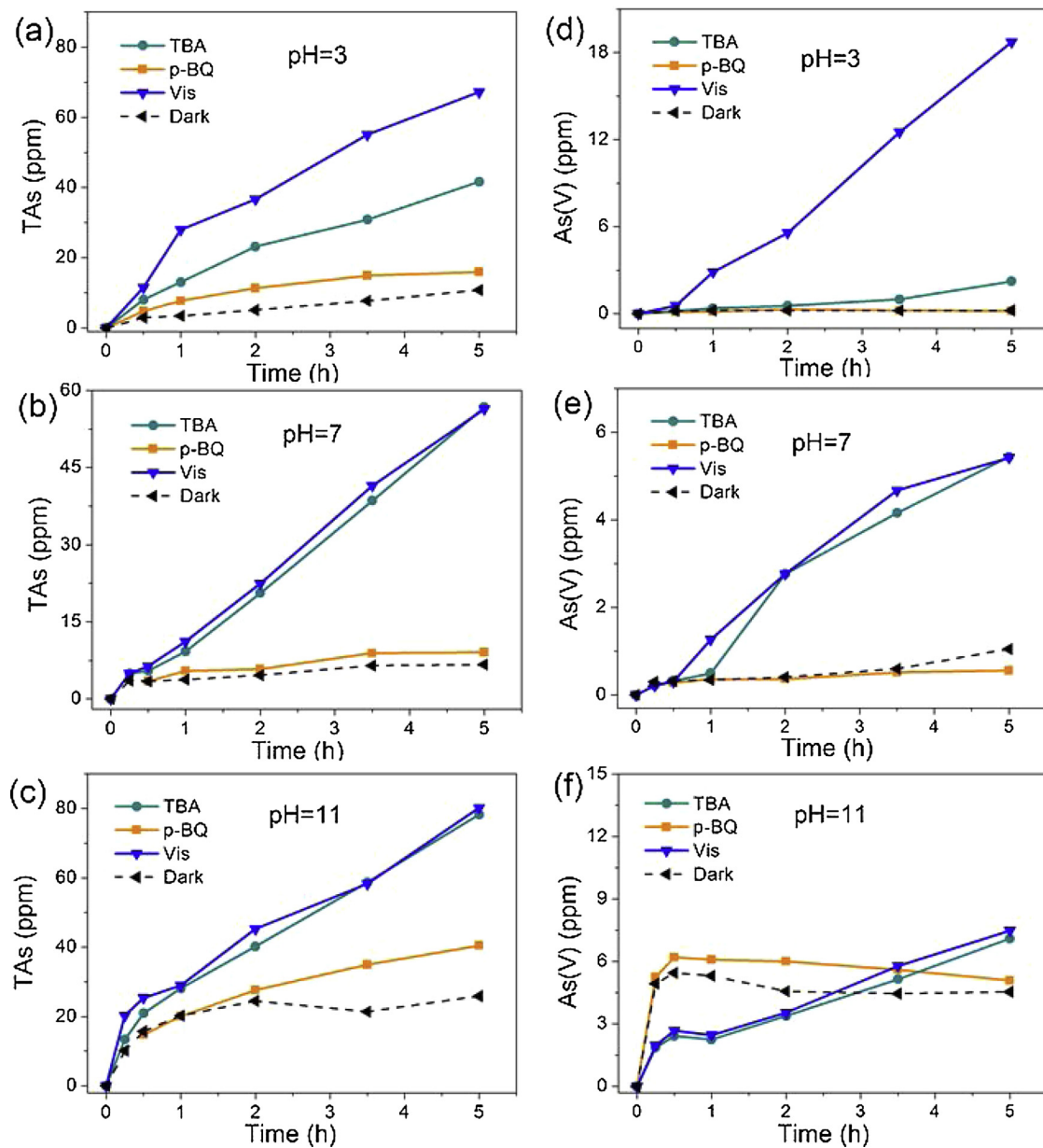
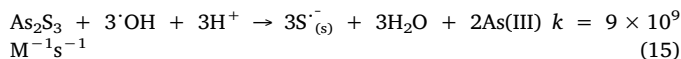


Fig. 6. Quenching effects of the radical scavengers, TBA and p-BQ, on the dissolution (a–c) and oxidation (d–f) of the sludge at different pHs.

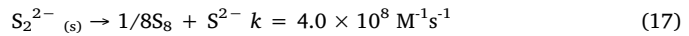
It has been reported that under light irradiation, sulfur radicals can be produced from the trapped photo-generated holes localized on the lattice sulfur ions with surface defects or impurities [42]. Therefore, it can be reasonably deduced that in our system, $\cdot\text{O}_2$ and $\cdot\text{OH}$ can react with the lattice sulfur on the surface of As_2S_3 to form sulfur-containing radicals, as described in Eqs. (14) and (15) [19,43].



During the photo-reaction process, As(III) can be released. The specific species of the released As(III) is highly dependent on the pH values and S^{2-} concentration. For example, H_3AsO_3 is the main species in the acid and neutral solution with little S^{2-} ions, while arsenic sulfide complexes, such as AsS_2 , HAs_2S_4 , $\text{H}_2\text{As}_3\text{S}_6$ and $\text{As(OH)}_x(\text{SH})_y^{3-x-y}$, form in the basic solution with a high concentration of S^{2-} [10–12].

The generation of sulfide containing radicals, $\text{S}^{\cdot-}_{(s)}$, will then transform into S_2^{2-} and finally produce S_8 , as presented in Eqs. (16) and

(17) [44].



Alternatively, $\text{S}^{\cdot-}_{(s)}$ can react with dissolving oxygen and convert to $\text{SO}_2^{\cdot-}$, and then quickly decompose to yield $\cdot\text{O}_2^-$, as described in Eqs. (18) and (19), which leads to the weak EPR signals of sulfur radicals detectable even at a very low temperature (Fig. 7a) [45].



3.10. The effects of intermediate sulfur species on the dissolution of ASS

During the dissolution of ASS under visible light, the intermediate sulfur species, such as S^{2-} , SO_3^{2-} and $\text{S}_2\text{O}_3^{2-}$, were detected in the system (Fig. 4). In order to understand the effect of these sulfur species

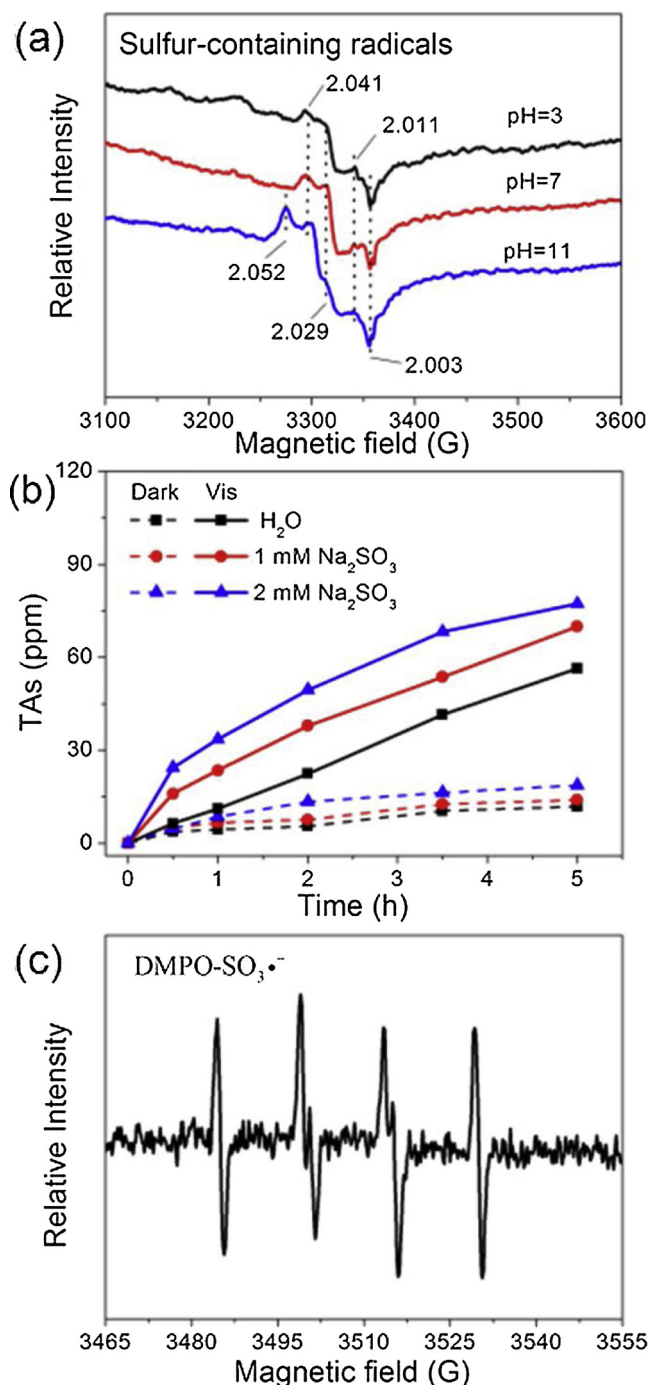
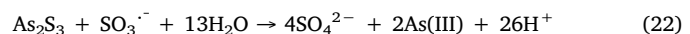


Fig. 7. (a) sulfur-containing radicals in the sludge by light irradiation for 10 min and annealing to 90 K. The numbers for peak position are g values. (b) Dissolution of the sludge (TAs) in sulfite solution under visible light at pH 7. (c) EPR spectrum of sulfite radical after 10 min reaction by adding 1 mM sulfite in the sludge system.

on the dissolution of ASS, extra sulfur-containing salts were employed into the system during illumination. As shown in Fig. 7b, when Na₂SO₃ was added, the dissolution of ASS was accelerated under light irradiation. The EPR result revealed that with the addition of Na₂SO₃ in the sludge, a new and strong signal of SO₃^{·-} [46] was observed under visible light (Fig. 7c). The generation of SO₃^{·-} was possibly from either photo-generated holes (eq 20) or hydroxyl radicals (Eq. (21)) [47].



The dissolution of ASS can be accelerated by SO₃^{·-}, as follows:



However, the addition of extra S²⁻ or S₂O₃²⁻ resulted in a decrease in dissolution rate of ASS (Fig. S8), where S²⁻ and S₂O₃²⁻ may act as the electron donors scavenging active oxygen species that contribute to the dissolution of ASS. Notably, no SO₄²⁻ was found in all the experimental systems mentioned above, which was verified by using methanol as the scavenger.

4. Conclusion

In the environment, a larger amount of arsenic sludge is discharged and deposited, especially during the treatment of acid mining and ore smelting wastewater. The sludge poses a major environmental threat, due to the potential release of arsenic ions. When the sludge is exposed to solar light irradiation, not only the release rate of As(III), but also the oxidation rate of As(III) to As(V) can be markedly accelerated, which will further increase the environmental risk of the discharged sludge. The mechanism of release and oxidation of As(III) from ASS accelerated by visible light is proposed as follows (Fig. 8). The ASS produces photo-generated holes (h_ν⁺) and electrons (e_{cb}⁻) under illumination, which will further react with the species (e.g. oxygen, hydroxide or sulfur) in solution to produce the corresponding active free radicals. O₂^{·-} is the primary free radical in the system, both for forming OH⁻ and sulfur-containing radicals and for releasing and oxidizing As(III) from ASS. At the higher pH (7 or 11), both the dissolution and the oxidation of the sludge are directly accelerated by O₂^{·-}. At the lower pH (3), the dissolution of the sludge is promoted by both O₂^{·-} and OH⁻, while the oxidation of As(III) is mainly by OH⁻. In the solid phase, the hydrophobic S₈ is formed on the surface of ASS through a series of sulfur radicals (S^{·(s)} and SO₂^{·-}) involved reactions, which favors the agglomeration and precipitation of ASS. In addition, the dissolution of ASS generates the intermediate sulfur species, in which SO₃²⁻ positively contributes to its dissolution by converting into SO₃^{·-} under visible light.

In order to check the dissolution and transformation of ASS in the environment, experiments were conducted under actual sunlight. Similar results were obtained as the simulated experiments, in which both the release of As(III) ions from ASS and the oxidation of As(III) into As(V) were accelerated by actual sunlight (see Fig. S9). The dissolution and oxidation rates of ASS under actual sunlight were much slower than those under simulated light, due to the unstable and weak intensity of actual sunlight. The finding in this work is meaningful to inform the development of an effective strategy for the safe stocking and treatment of slag residue. In addition, the photochemical reactions on the ASS can generate active oxygen and sulfur species under light illumination. These entities will not only affect the migration and transformation behaviors of heavy metals ions and organic compounds in the environment, but also interfere with the geochemical cycle process of the important elements, such as sulfur. Further studies on limiting the dissolution and oxidation of the deposited ASS in natural environments, and/or the development of methods to extract arsenic for detoxifying the sludge and resource recycling, are required to support future improvements in environmental management at relevant industry sites.

Acknowledgements

The authors acknowledge the financial support from National Key Research and Development Program of China (2017YFA0207204 and 2016YFA0203101), the National Natural Science Foundation of China (Grant No. 21876190 and 21836002), the Key Research and Development Program of Ningxia (2017BY064), and the “One Hundred Talents Program” in Chinese Academy of Sciences.

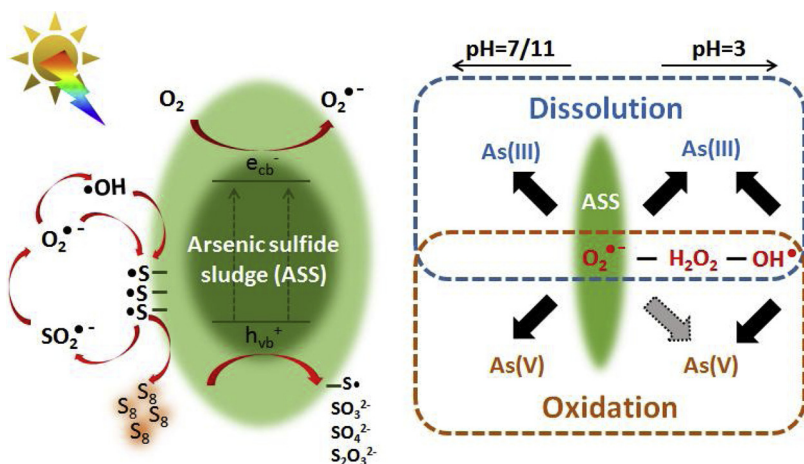


Fig. 8. Conceptual model of the photocatalytic dissolution and oxidation of arsenic sulfide sludge.

Appendix A. Supplementary data

Supplementary material related to this article can be found, in the online version, at doi:<https://doi.org/10.1016/j.apcatb.2019.03.020>.

References

- [1] W.R. Cullen, K.J. Reimer, *Chem. Rev.* 89 (1989) 713–764.
- [2] P.A. Riveros, J.E. Dutrizac, P. Spencer, *Can. Metall. Quart.* 40 (2001) 395–420.
- [3] H.E. Jamieson, *Rev. Mineral. Geochem.* 79 (2014) 533–587.
- [4] R.P. Liu, Z.C. Yang, Z.L. He, L.Y. Wu, C.Z. Hu, W.Z. Wu, J.H. Qu, *Chem. Eng. J.* 304 (2016) 986–992.
- [5] L. Kong, X. Peng, X. Hu, *Environ. Sci. Technol.* 51 (2017) 12583–12591.
- [6] A. Lewis, R. Van Hille, *Hydrometallurgy* 81 (2006) 197–204.
- [7] L. Guo, Y. Du, Q. Yi, D. Li, L. Cao, D. Du, *Sep. Purif. Technol.* 142 (2015) 209–214.
- [8] A. Bhattacharya, J. Routh, G. Jacks, P. Bhattacharya, M. Morth, *Appl. Geochem.* 21 (2006) 1760–1780.
- [9] L.E. Eary, *Geochim. Cosmochim. Acta* 56 (1992) 2267–2280.
- [10] R.M. Florouli, A.P. Davis, A. Torrents, *Environ. Sci. Technol.* 38 (2004) 1031–1037.
- [11] S. Stauder, B. Raue, F. Sacher, *Environ. Sci. Technol.* 39 (2005) 5933–5939.
- [12] R.T. Wilkin, D. Wallschlaeger, R.G. Ford, *Geochem. T.* 4 (2003) 1–7.
- [13] X. Hu, L. Kong, M. He, *Environ. Sci. Technol.* 48 (2014) 14266–14272.
- [14] X.Y. Hu, M.C. He, L.H. Kong, *Appl. Geochem.* 61 (2015) 53–61.
- [15] X.Y. Hu, X.J. Peng, L.H. Kong, *Environ. Sci. Technol.* 52 (2018) 1954–1962.
- [16] G. Mills, Z.G. Li, D. Meisel, *J. Phys. Chem.* 92 (1988) 822–828.
- [17] S. Hu, J.S. Lu, C.Y. Jing, *J. Environ. Sci.* 24 (2012) 1341–1346.
- [18] J.D. Cline, *Limnol. Oceanogr.* 14 (1969) 454–458.
- [19] J. Zhu, K. Petit, A.O. Colson, S. Debolt, M.D. Sevilla, *J. Phys. Chem.* 95 (1991) 3676–3681.
- [20] O. Kondrat, R. Holomb, A. Csik, V. Takats, M. Veres, V. Mitsa, *Nanoscale Res. Lett.* 12 (2017) 149.
- [21] D.S. Han, B. Batchelor, A. Abdel-Wahab, *J. Colloid Interface Sci.* 368 (2012) 496–504.
- [22] H. Chen, Z.L. Zhang, Z.L. Yang, Q. Yang, B. Li, Z.Y. Bai, *Chem. Eng. J.* 273 (2015) 481–489.
- [23] A.C. Scheinost, R. Kirsch, D. Banerjee, A. Fernandez-Martinez, H. Zaenker, H. Funke, L. Charlet, *J. Contam. Hydrol.* 102 (2008) 228–245.
- [24] W.M. Liu, S. Chen, *Wear* 238 (2000) 120–124.
- [25] M. Sadiq, T.H. Zaidi, A.A. Mian, *Water Air Soil Pollut.* 20 (1983) 369–377.
- [26] X. Peng, J. Chen, L. Kong, X. Hu, *Environ. Sci. Technol.* 52 (2018) 4794–4801.
- [27] M.F. Lengke, R.N. Tempel, *Geochim. Cosmochim. Acta* 65 (2001) 2241–2255.
- [28] X. Xu, R.J. Lu, X.F. Zhao, Y. Zhu, S.L. Xu, F.Z. Zhang, *Appl. Catal. B Environ.* 125 (2012) 11–20.
- [29] B. Luo, D. Xu, D. Li, G. Wu, M. Wu, W. Shi, M. Chen, *ACS Appl. Mat. Interfaces* 7 (2015) 17061–17069.
- [30] J.G. Guo, Y. Liu, Y.J. Hao, Y.L. Li, X.J. Wang, R.H. Liu, F.T. Li, *Appl. Catal. B Environ.* 224 (2018) 841–853.
- [31] J.C. Wang, J. Ren, H.C. Yao, L. Zhang, J.S. Wang, S.Q. Zang, L.F. Han, Z.J. Li, *J. Hazard. Mater.* 311 (2016) 11–19.
- [32] J. Wang, W.J. Jiang, D. Liu, Z. Wei, Y.F. Zhu, *Appl. Catal. B Environ.* 176 (2015) 306–314.
- [33] J.C. Sin, S.M. Lam, I. Satoshi, K.T. Lee, A.R. Mohamed, *Appl. Catal. B Environ.* 148 (2014) 258–268.
- [34] Z. Zhang, F. Yu, L. Huang, J. Jiatiel, Y. Li, L. Song, N. Yu, D.D. Dionysiou, *J. Hazard. Mater.* 278 (2014) 152–157.
- [35] X.H. Jiang, Q.J. Xing, X.B. Luo, F. Li, J.P. Zou, S.S. Liu, X. Li, X.K. Wang, *Appl. Catal. B Environ.* 228 (2018) 29–38.
- [36] P.S. Rao, E. Hayon, *J. Phys. Chem.* 79 (1975) 397–402.
- [37] M. Sun, G. Zhang, Y. Qin, M. Cao, Y. Liu, J. Li, J. Qu, H. Liu, *Environ. Sci. Technol.* 49 (2015) 9289–9297.
- [38] B. Jiang, J. Guo, Z. Wang, X. Zheng, J. Zheng, W. Wu, M. Wu, Q. Xue, *Chem. Eng. J.* 262 (2015) 1144–1151.
- [39] H. Lee, W. Choi, *Environ. Sci. Technol.* 36 (2002) 3872–3878.
- [40] J. Ryu, W. Choi, *Environ. Sci. Technol.* 38 (2004) 2928–2933.
- [41] S. Yanagida, K. Mizumoto, C. Pac, *J. Am. Chem. Soc.* 108 (1986) 647–654.
- [42] K.C. Khulbe, R.S. Mann, *Zeitschrift Fur Physikalische Chemie-Leipzig* 271 (1990) 1263–1270.
- [43] R. Wedmann, S. Bertlein, I. Macinkovic, S. Boltz, J. Miljkovic, L.E. Munoz, M. Herrmann, M.R. Filipovic, *Nitric Oxide* 41 (2014) 85–96.
- [44] C.A. Linkous, C.P. Huang, J.R. Fowler, *J. Photochem. Photobiol. A-Chem.* 168 (2004) 153–160.
- [45] T.N. Das, R.E. Huie, P. Neta, S. Padmaja, *J. Phys. Chem. A* 103 (1999) 5221–5226.
- [46] K. Rangelova, A.B. Rice, A. Khajo, M. Triquigneaux, S. Garantiotis, R.S. Maggiozzo, R.P. Mason, *Free Radic. Biol. Med.* 52 (2012) 1264–1271.
- [47] J. Zhang, L. Zhu, Z. Shi, Y. Gao, *Chemosphere* 186 (2017) 576–579.